Atomically Resolved Images of I_h Ice Single Crystals in the Solid Phase

Keita Kobayashi, Masanori Koshino, and Kazu Suenaga*

Nanotube Research Center, National Institute of Advanced Industrial Science and Technology (AIST), Tsukuba 305-8565 Japan

(Received 25 January 2011; published 16 May 2011)

The morphology and crystal structure of nanoparticles of ice were examined by high-resolution transmission electron microscopy. Two different crystal structures were found and unambiguously assigned to hexagonal (I_h) and cubic (I_c) ice crystals. Direct observation of oxygen columns clearly revealed the hexagonal packing of water molecules. Electron energy-loss spectroscopy was used to monitor the electronic excitation in ice, suggesting possible dissociation of water molecules. Dynamic process of phase transition between I_h and I_c phases of individual ice nanoparticles under electron beam irradiation was also monitored by *in situ* transmission electron diffractometry.

DOI: 10.1103/PhysRevLett.106.206101 PACS numbers: 68.37.Og, 61.46.Hk, 73.22.Dj, 96.50.Dj

Water is one of the most abundant substances on Earth, and is crucial to all known living creatures. Direct visualization of water molecules and their various configurations would be of general interest. Ice, water in its solid state, is known to exhibit polymorphic structures, depending on the environmental conditions [1]. Ice exists even in outer space, in comet clouds and interstellar grains [2,3], and therefore its morphology and crystal structure are of great importance for space scientists. Considerable effort has been devoted to exploring the phase transitions and the various structures of condensed water molecules at low temperature, using crystallographic diffraction [3–7] and thermal analytical methods [6–8]. Nevertheless, most structural studies have been performed on bulk ice aggregates with averaged structures, and the morphology of ice crystals has so far not been investigated in detail at the nanometer scale.

In addition, electronic excitation by ionizing radiation in water is important in biological tissue, because it can lead to the dissociation of water molecules. The resulting plasmonic behavior can transfer energy to nearby molecules in an ion channel-like effect. Optical absorption and electron energy-loss spectroscopy (EELS) studies of water in solid and gas phases have been reported [9–13], but none of these studies were performed on individual ice crystals of nanometer scale. EELS of individual ice crystals with known morphology and crystal structure has never been reported.

Transmission electron microscopy (TEM) of ice has also been largely unreported, except for a few low-magnification observations [7,14] and simple lattice fringe analysis [15]. In particular, water molecules have never been visualized directly in the solid phase using high-resolution transmission electron microscopy (HRTEM). This is because HRTEM studies of small-molecule crystals such as water are hampered by intrinsic problems during observation. Hydrogen bonds and van der Waals interactions are relatively weak compared to the covalent or metallic bonds of materials commonly observed using TEM, and therefore the incident electron beam can induce severe damage by breaking these bonds. Knock-on damage is not negligible for TEM observation of ice [5]. Because the maximum threshold energy of the hydrogen atom under 120 kV electron irradiation is estimated to ~290 eV [16], any bonds weaker than this (the typical bond-dissociation energy of OH^- into H and O^- is 4.8 eV) may suffer from knock-on damage. The treatment of knock-on damage for water must also be considered with caution, because the energy imparted from electrons to hydrogen could also be converted into motion. Moreover, high current density electron beam irradiation in HRTEM generates heat at the sample, and the ice particles can readily sublimate. Indeed, lowering the temperature of the TEM grid is necessary to maintain solid water at low pressure. For example, the sublimation point of ice is ~148 K at 10^{-5} Pa [17]. Hence, visualizing such a low-molecular weight substance by HRTEM remains a challenge. In this study, we prepare well-crystallized ice nanoparticles within a TEM column, and demonstrate successful HRTEM and EELS studies on the individual ice nanoparticles.

Water ice nanoparticle specimens were prepared as follows. A TEM micro grid, wetted with distilled methanol, was held in a cryo-holder (Gatan, Model 626DH J5 UPR). The grid was quenched by dipping tip of the cryo-holder into liquid nitrogen, and subsequently the cryo-holder was cooled by supplying liquid nitrogen. The grid was then exposed to a moist atmosphere with a specific water vapor pressure of 1.2 kPa and a temperature of 298.8 K, for 20 s. The specimen was then directly introduced into a TEM column (vacuum: ~10^{-5} Pa) keeping the low temperature. Although crystalline ice nanoparticles can also be prepared on TEM grids without methanol pretreatment, ice nanoparticles with smaller diameter could be grown on pretreated TEM grids [18]. The coexistence of methanol and water vapor mimics the conditions in comet clouds, although the effect of the methanol partial pressure on the morphology of ice nanoparticles remains unclear.

 © 2011 American Physical Society

HRTEM observation of the specimens was carried out using a JEM-2010F/UHR (JEOL), equipped with a post-specimen spherical aberration corrector (CEOS, typical C_S values of ~ 3 μm), and operated at an accelerating voltage of 120 kV. This instrument has the point resolution better than 0.106 nm [19] and therefore capable to resolve the oxygen column of hexagonal ice crystal, which is typically separated by 0.25 nm. An ENFINA 100 (Gatan) was used for EELS chemical/valence analysis on the same equipment. All the HRTEM and EELS experiments were performed at ~ 95 K and a pressure of $\sim 10^{-5}$ Pa. Since the ice nanoparticles almost instantly evaporated under the incident electron beam, the exposure time for image recording was minimized to 0.5 s, from a very thin region with a rapidly moving and evaporating frontier. The typical electron dose under imaging conditions of low-magnification TEM images (Figs. 1) and HRTEM images (Figs. 2) was estimated as $\sim 1.0 \times 10^2$ and $\sim 6.7 \times 10^4$ electrons/nm^2 frame, respectively. Phase transition of an isolated ice nanoparticle under electron beam irradiation was also monitored by *in situ* transmission electron diffractometry (TED) with a constant dose rate of 4.8×10^3 electron/nm^2 s. A smallest selected area aperture (200 nm in diameter) was used to obtain the information from a specific ice particle for TED and EELS measurements.

TEM observation shows an abundance of particles dispersed on the TEM grid in the micro- to nanosize range [18]. TED analysis of individual particles indicates that those exhibiting well-developed facets are single crystals, whereas rounded particles without facets are polycrystalline. The distribution of particle size with the degree of faceting and typical TEM images of these particles (inset) are shown in Figs. 1(a) and 1(b). The diameter-distribution histogram of the rounded particles [Fig. 1(a)] shows a diameter range from 60 to 1400 nm (The mean diameter ($\bar{d}$) = 390 nm, standard deviation (σ) = 300 nm). Similarly, Fig. 1(b) shows that the diameter of the faceted particles ranges from 240 to 2400 nm ($\bar{d}$ = 800 nm, σ = 580 nm). These histograms clearly show that the faceted particles tend to exhibit larger diameter than the rounded particles. Additionally, further EELS chemical analysis of individual particles confirms the existence of oxygen with no trace of carbon.

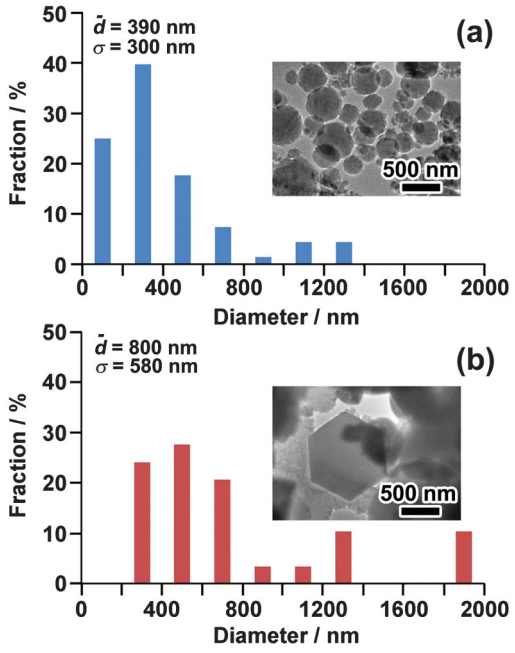

FIG. 1 (color). (a),(b) Histograms of the diameter-distribution of rounded and faceted particles, suggesting that ice particles with larger diameter tend to be faceted. (inset) Typical corresponding low-magnification TEM images of the particles.

TED and HRTEM observations reveal that the ice specimen is a mixture of the ice particles with I_h symmetry and with cubic symmetry (ice I_c) (Details are shown in supplemental materials [18]). Figure 2(a) shows a typical HRTEM image of a relatively stable ice nanoparticle taken from a [0001] zone axis of a I_h phase. In this image one can see the bright dots regularly separated by ~ 0.25 nm, which precisely coincides with the distance of oxygen columns in the observed direction. TEM image simulation of ice I_h [Fig. 2(b)] indeed shows similar bright dots at the oxygen column positions in several defocus conditions [18,20]. Direct comparison of the experimental HRTEM image with the simulation should not be simply done yet. There are three factors that can alter the HRTEM image; (i) the

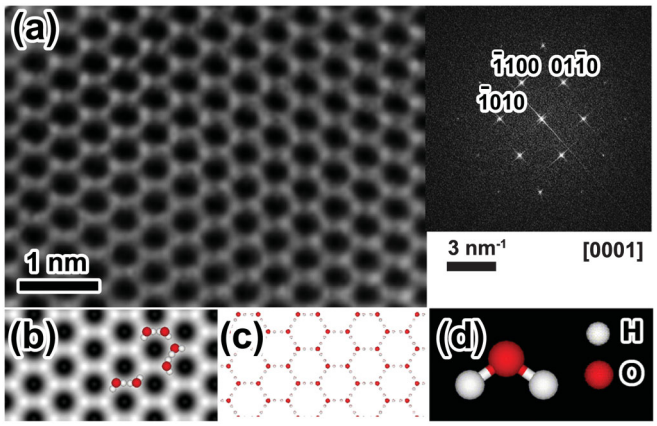

FIG. 2 (color). (a) HRTEM and corresponding FFT pattern of an ice nanoparticle with ice I_h structure. The image shows the hexagonal network shown as bright dots, which are separated by ~ 0.25 nm. (b) Simulated TEM image viewed from the [0001] zone axis of ice I_h using the following parameters: convergence angle of 0.5 mrad, C_S value of 3 μm, defocus spread of 9 nm, sample thickness of 42 nm, defocus value of +33 nm (overfocus), and objective aperture radius of 7 nm^{-1}. The simulation image shows bright dots, which corresponds to the position of the oxygen columns. Models of water molecules are superimposed. (c) A crystal model of the [0001] zone axis of ice I_h. Hydrogen atoms (white circles) are located between the oxygen columns (red circles), but are invisible in experiment. (d) Schematic model of a water molecule.

nonlinear imaging effect, (ii) the dynamical contributions and (iii) the off-centered optic axis, none of which was considered in our simulation. Also the thickness of the examined particle and the defocus value cannot be accurately determined because of its rapid vaporization process which does not allow us a full set of through-focus imaging. Nevertheless it is clear that the regularly separated bright dots should reflect the hexagonal network of oxygen columns.

As seen in the water crystal model [Fig. 2(c)], hydrogen atoms (white circles) should be located between the oxygen columns (red circles). Our method is not able to visualize these hydrogen atoms, mainly because of their extremely weak scattering power. Additionally, at 95 K, the water molecules are expected to be rotating, and only two of the four sites should be occupied by hydrogen atoms [21]. Therefore there is some uncertainty in the detection of the hydrogen atom positions. A schematic model of a water molecule is shown in Fig. 2(d).

Electron microscopy has recently begun to be able to visualize the light elements such as B, C, N, and O [22]. However, the materials studied by the modern electron microscopes were so far limited to the very specific or artificial specimens such as graphene or *h*-BN single sheet, which are definitely suited to these experiments because they are atomically thin and very stable under the electron beam. Application to the realistic or general materials has been hardly reported. Especially electron beam sensitive materials with low-z elements are believed to be very difficult to image atomically. This is the first successful observation of the oxygen column in solid water. Indeed, ice is a lightest substance in terms of density ($\sim 0.92\ \mathrm{g\,cm^{-3}}$ at atmospheric pressure and 98 K [1]) that has ever visualized its atomic structure by HRTEM.

EELS on a single nanoparticle of ice is shown in Fig. 3. An overall energy region for core-loss spectroscopy is shown in Fig. 3(a). This spectrum clearly proves the absence of carbon and the presence of oxygen, and therefore the ice nanoparticles cannot be confused with the minor product of solidified methanol. Valence loss EELS [Fig. 3(b)] can be compared with absorption or near-edge x-ray absorption fine structure spectroscopy [23]. The typical features are small, but visible peaks at 8.8, 10.6, and 14.5 eV are assigned to interband transitions [24]. The peak at 21 eV is often attributed to the bulk plasmon [25,26], while the peak at 19 eV may be due to photoabsorption of an ionic state, H_2O^+ [27,28]. The peak at 17 eV may be attributed to the surface plasmon mode, but as yet is not fully assigned.

EELS simulation was performed to corroborate the oxygen *K* edge [Fig. 3(c)] [18]. The simulated spectra do not show an exact match to the experiment, because the experimental oxygen *K* edge shows a shoulder peak just before the main peak at ~546 eV, which is not completely reproduced for ice I_c or ice I_h spectra by the simulation.

This discrepancy is quite interesting and reflects the intrinsic difficulty of EELS core-loss spectroscopy at high spatial resolution on a light molecular crystal. The loss of hydrogen atoms due to the dissociation effect is inevitable, and the O-H bond might be easily broken under the 120 kV electron beam [5,29]. Also, the rapid vaporization process may induce some changes in energy-loss

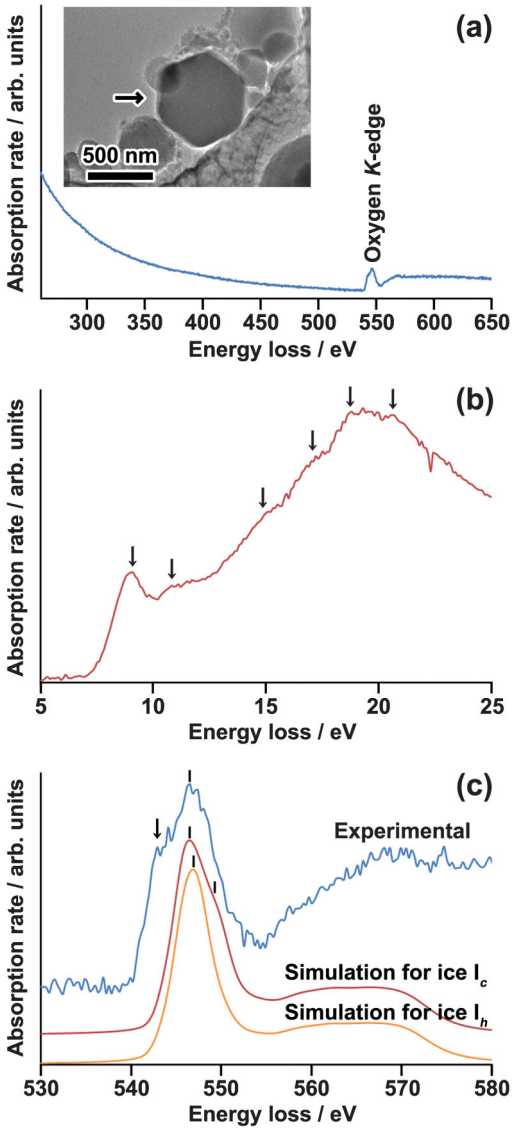

FIG. 3 (color). (a) Core-level EELS from an individual ice nanoparticle, showing the oxygen *K*-edge (~ 540 eV). Note that no carbon *K* edge can be detected. (inset) TEM image of the corresponding ice nanoparticle (indicated by an arrow) (b) EELS valence analysis of a hexagonal ice nanoparticle. The interband transitions are quite visible and specific to crystalline ice particles. The peak at 21 eV is a bulk plasmon. (c) Oxygen *K*-edge fine structure of the experimental and simulated spectra. The prepeak (~ 542 eV) just before the main peak (546 eV) of the experimental spectrum cannot be reproduced by simulations for ice I_h or I_c. A smallest selected area aperture (200 nm in diameter) was used.

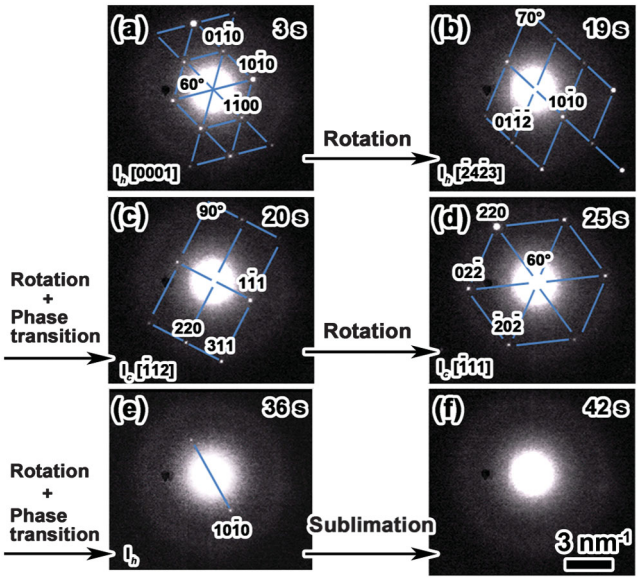

FIG. 4 (color). Sequential TED patterns of an isolated ice nanoparticle recorded at a constant dose rate with 4.8×10^3 electrons/nm^2 s. (a)–(f) 3, 19, 20, 5, 36, and 42 s, respectively.

near-edge structure, involving melting of the ice surface. It is speculated that such ionization or radiation-related phenomena would also happen to ice particles in outer space by cosmic rays.

Figures 4(a)–4(h) show sequential *in situ* TED patterns of an individual ice nanoparticle during structural evolutions. The changes can be interpreted as a mixture of the phase transition (between I_h and I_c) and a rotation of the nanoparticle in respect to the electron beam. The pristine ice nanoparticle retains the I_h phase [Fig. 4(a)] until 6 s exposure. Then the TED patterns continuously alter with the increasing electron irradiation time, which is attributed to the phase transitions of the ice nanoparticle from I_h [Figs. 4(a) and 4(b)] to I_c [Figs. 4(c) and 4(d)] with rotations of the particle. After another phase transition from I_c to I_h [Fig. 4(e)], the ice nanoparticle eventually sublimates [Fig. 4(f)] (Details are shown in the supplemental material [18]). Although Heide and Zeitler [14] have reported that I_c phase tends to alter to I_h over 100 K under an electron beam irradiation, such a reversible phase transition between I_h to I_c have never been reported at the observed temperature ($\sim$ 95 K). Since the energy levels of both phases are so close (the latent heat of the phase transition between ice I_h and I_c is estimated as small as 113 J/mol [1,30]), the reversible phase transition may be reasonable under electron microscopic observation.

In this study, we demonstrated the analysis of solid water nanoparticles by HRTEM and EELS fine structures. Morphology and spectroscopic information, together with atomic configuration, are now accessible on individual nanoparticles. Future observations using this technique of ice particles transferred directly from outer space would be extremely intriguing.

This study has been supported by the JST CREST program and Grant-in-Aid for Scientific Research (No. 19054017).

*suenaga-kazu@aist.go.jp

[1] N. H. Fletcher, *The Chemical Physics of Ice* (Cambridge Univ. Press, Cambridge, 1970).
[2] D. A. Rothery, *Satellites of the Outer Planets* (Oxford Univ. Press, Oxford, 1992).
[3] H. Fukazawa *et al.*, Astrophys. J. **652**, L57 (2006).
[4] H. König, Z. Kristallogr. **105**, 279 (1944).
[5] H.-G. Heide, Ultramicroscopy **14**, 271 (1984).
[6] A. J. Leadbetter *et al.*, J. Chem. Phys. **82**, 424 (1985).
[7] P. Jenniskens *et al.*, J. Chem. Phys. **107**, 1232 (1997).
[8] S. Kawada, J. Phys. Soc. Jpn. **32**, 1442 (1972).
[9] C. D. Wilson, C. A. Dukes, and R. A. Baragiola, Phys. Rev. B **63**, 121101(R) (2001).
[10] R. I. Platzman, in *Radiation Research*, edited by G. Silini (North-Holland, Amsterdam, 1967).
[11] J. Daniels, Opt. Commun.**3**, 240(1971).
[12] J. M. Heller, R. N. Hamm, R. D. Birkhoff, and L. R. Painter, J. Chem. Phys. **60**, 3483 (1974).
[13] G. R. Wight and C. E. Brion, J. Electron Spectrosc. Relat. Phenom. **4**, 25 (1974).
[14] H.-G. Heide and E. Zeitler, Ultramicroscopy **16**, 151 (1985).
[15] M. Cyrklaff and W. Kühlbrandt, Ultramicroscopy **55**, 141 (1994).
[16] L. W. Hobbs, in *Introduction to Analytical Electron Microscopy*, edited by J. J. Hren, J. I. Goldstein, and D. C. Joy (Plenum Press, New York, 1979), p. 437.
[17] in *Vacuum Handbook*, edited by ULVAC, Inc. (Ohmsha, Tokyo, 2002).
[18] See supplemental material at http://link.aps.org/supplemental/10.1103/PhysRevLett.106.206101 for additional data.
[19] Z. Liu, K. Suenaga, P. J. F. Harris, and S. Iijima, Phys. Rev. Lett.**102**, 015501 (2009).
[20] A. Goto, T. Hondoh, and S. Mae, J. Chem. Phys. **93**, 1412 (1990).
[21] L. Pauling, J. Am. Chem. Soc. **57**, 2680 (1935).
[22] O. L. Krivanek *et al.*, Nature (London) **464**, 571 (2010).
[23] M. Seki, K. Kobayashi, and J. Nakahara, J. Phys. Soc. Jpn. **50**, 2643 (1981).
[24] K. Kobayashi, J. Phys. Chem. **87**, 4317 (1983).
[25] M. Zaider, J. L. Fru, and D. E. Orr, Radiation Protection Dosimetry **31**, 23 (1990).
[26] J. A. LaVerne and A. Mozumder, Radiat. Res. **133**, 282 (1993).
[27] L. C. Lee and M. Suto, Chem. Phys. **110**, 161 (1986).
[28] K. F. Dunn, P. F. O'Neill, R. Browning, C. R. Browne, and C. J. Latimer, J. Electron Spectrosc. Relat. Phenom. **79**, 475 (1996).
[29] E. Knapek, G. Lefranc, H. G. Heide, and I. Dietrich, Ultramicroscopy**10**, 105(1982).
[30] R. H. Beaumont, H. Chihara, and J. A. Morrison, J. Chem. Phys. **34**, 1456(1961).